HHS Public Access

Author manuscript

Nat Commun. Author manuscript; available in PMC 2016 January 16.

Published in final edited form as:

Nat Commun. ; 6: 7768. doi:10.1038/ncomms8768.

D2HGDH regulates alpha-ketoglutarate levels and dioxygenase function by modulating IDH2

An-Ping Lin[1], **Saman Abbas**[1], **Sang-Woo Kim**[1], **Manoela Ortega**[1], **Hakim Bouamar**[1], **Yissela Escobedo**[1], **Prakash Varadarajan**[1], **Yuejuan Qin**[1], **Jessica Sudderth**[6], **Eduard Schulz**[2], **Alexander Deutsch**[2], **Sumitra Mohan**[3], **Peter Ulz**[3], **Peter Neumeister**[2], **Dinesh Rakheja**[5], **Xiaoli Gao**[4], **Andrew Hinck**[4], **Susan T. Weintraub**[4], **Ralph J. DeBerardinis**[6], **Heinz Sill**[2], **Patricia L. M. Dahia**[1,7,8], and **Ricardo C.T. Aguiar**[1,7,8,9]

[1]Division of Hematology and Medical Oncology, Department of Medicine, University of Texas Health Science Center at San Antonio, San Antonio, Texas, 78229, USA

[2]Division of Hematology, Medical University of Graz, Graz, A-8036, Austria

[3]Institute of Human Genetics, Medical University of Graz, Graz, A-8036, Austria

[4]Department of Biochemistry, University of Texas Health Science Center at San Antonio, San Antonio, Texas, 78229, USA

[5]Departments of Pathology and Pediatrics, University of Texas Southwestern Medical Center and Children's Medical Center, Dallas, Texas 75390, USA

[6]Department of Pediatrics, Children's Medical Center Research Institute at University of Texas Southwestern, Dallas, Texas 75390, USA

[7]Greehey Children's Cancer Research Institute, University of Texas Health Sciences Center at San Antonio, San Antonio, Texas, 78229, USA

[8]Cancer Therapy and Research Center, University of Texas Health Science Center at San Antonio, San Antonio, Texas, 78229, USA

[9]South Texas Veterans Health Care System, Audie Murphy VA Hospital, San Antonio, San Antonio, Texas, 78229, USA

Abstract

Correspondence to: Ricardo Aguiar, MD PhD, Department of Medicine, University of Texas Health Science Center at San Antonio, 7703 Floyd Curl Drive, San Antonio, TX, 78229, Phone: 1-210-567-4860, aguiarr@uthscsa.edu.

Author Contributions: Author Contributions: A-P. L., S.A. and S-W.K generated critical reagents, conducted experiments and analysed data; M.O. conducted experiments; H.B. helped with the FACS analyses; Y.E. and P.V. conducted *D2HGDH*, *L2HGDH*, and *IDH1/2* amplification for sequencing; Y.Q. performed the immunofluorescence staining; E.S. and A.D. conducted D2HGHD amplification and sequencing analysis; S. M. and P. U. performed the copy number analysis; P.N. provided well-characterized patient samples; X.G., D.R. and S.W. conducted mass spectrometry studies; A.H. created the structural models for D2HGDH; J.S performed glutamine tracing studies; R.D. designed and coordinated the glutamine tracing studies, and analyzed data; H.S. provided well-characterized patient samples and analysed data; P.L.M.D. coordinated the sequencing component of the study, designed assays and analysed data; R.C.T.A designed and coordinated the study, conducted experiments, analysed data and wrote the manuscript, which was reviewed by all authors.

The authors have no conflict of interest to declare

Isocitrate dehydrogenases (IDH) convert isocitrate to alpha-ketoglutarate (α-KG). In cancer, mutant IDH1/2 reduces α-KG to D2-hydroxyglutarate (D2-HG) disrupting α-KG-dependent dioxygenases. However, the physiological relevance of controlling the interconversion of D2-HG into α-KG, mediated by D2-hydroxyglutarate dehydrogenase (D2HGDH), remains obscure. Here we show that wild-type D2HGDH elevates α-KG levels, influencing histone and DNA methylation, and HIF1α hydroxylation. Conversely, the D2HGDH mutants that we find in diffuse large B-cell lymphoma are enzymatically inert. D2-HG is a low-abundance metabolite, but we show that it can meaningfully elevate α-KG levels by positively modulating mitochondrial IDH activity and inducing IDH2 expression. Accordingly, genetic depletion of IDH2 abrogates D2HGDH effects, whereas ectopic IDH2 rescues D2HGDH-deficient cells. Our data link D2HGDH to cancer and describe an additional function for the enzyme: the regulation of IDH2 activity and α-KG-mediated epigenetic remodeling. These data further expose the intricacies of mitochondrial metabolism and inform on the pathogenesis of D2HGDH-deficient diseases.

Isocitrate dehydrogenases (IDH) catalyze the reversible conversion of isocitrate to alpha-ketoglutarate (α-KG). Mutant IDH1/2 creates a neomorphic enzyme that reduces α-KG to the structurally related D2-hydroxyglutarate (D2-HG)[1–3]. This metabolic deregulation impinges on the activity of multiple α-KG dependent dioxigenases[4], and induces epigenetic changes that are proposed to play a role in the pathogenesis of IDH1/2 mutant cancers[5–7]. These observations also suggest the need for a tight physiological control of the cellular levels of α-KG and D2-HG. The interconversion of D2-HG into α-KG is mediated by D2-hydroxyglutarate dehydrogenase (D2HGDH)[8]. Under normal conditions, D2-HG is considered an unwanted byproduct of cellular metabolism with no known physiologic role. Thus, the current thought is that D2HGDH primarily functions to prevent the potentially deleterious cellular accumulation of D2-HG[9]. In agreement with this concept, loss-of-function mutation and deletion of *D2HGDH* causes a severe autosomal recessive neurometabolic disorder, type I D-2-hydroxyglutaric aciduria (D-2-HGA)[10]. However, the relevance of D2HGDH's activity to mitochondrial metabolism and its putative ability to promote an oncogenic metabolic deregulation remains underexplored.

There are two possible enantiomers of 2-HG. In addition to D2-HG which in converted to α-KG by D2HGDH, there is L2-HG, which has its cellular accumulation prevented by the activity of the dehydrogenase L2HGDH[10]. Similarly to D2HGDH, hereditary loss of L2HGDH also causes a neurometabolic disorder with an autosomal recessive mode of inheritance, L-2-Hydroxyglutaric aciduria (L-2-HGA)[11,12]. Interestingly, patients diagnosed with L-2-HGA appear to be at a higher risk of developing brain tumours than matching control populations[13]. Further, recent evidence has implicated reduced expression of L2HGDH as a somatic event in renal cell carcinoma, which resulted in dioxygenase-related epigenetic deregulation[14]. Thus, in addition to the accumulation of D2-HG in IDH1/2 mutant tumours, the related metabolite, L2-HG, has also been linked to cancer. In both instances, the resulting metabolic imbalance yielded an epigenetic phenotype that was related to the deregulation of α-KG-dependent dioxygenase. These observations suggest that an in-depth examination of this metabolic axis is warranted in diseases associated with significant epigenetic remodelling.

The elucidation of the genetic landscape of diffuse large B cell lymphoma (DLBCL) highlighted a previously unappreciated role of epigenetic modifiers in the pathogenesis of this disease. Regulators of histone methylation and acetylation, as well as DNA methylation, including MLL2, EZH2, CREBBP, EP300, TET2 and TET1, have been found to be somatically mutated, deleted or epigenetically silenced in these tumours[15–20]. Concrete evidence for the importance of these epigenetic modifiers to B cell lymphoma biology has also been mounting. Aberrant lymphoid differentiation has been reported in Tet2 null mice[19], and frank B cell lymphoma has been recently described upon deletion of Tet1 in vivo[20]. These observations are relevant in the context of the present work because a significant fraction of the enzymes that regulate histone and DNA methylation (e.g., Jumonji histone demethylases and TET DNA hydroxylases) belong to the family of α-KG-dependent dioxygenases, which can be functionally inactivated by α-KG-related metabolic imbalances. Thus, although mature B cell malignancies do not harbor D2-HG producing *IDH1/IDH2* mutations[21], the presence of other genetic defects, such as loss of D2HGDH, that may cause actual or relative (competitive) α-KG deficiency and aberrant epigenetic remodelling has not been examined in depth.

Here we show that somatic, truncating and missense, heterozygous *D2HGDH* mutations are present in a small subset of DLBCL. The DLBCL-associated *D2HGDH* mutations target the same protein domains disrupted in the autosomal recessive type I D-2-HGA. Detailed enzymatic and cellular examination defined these variants as loss- of-function. The principal consequence of the partial loss of D2HGDH in DLBCL is a significant decrease in the cellular levels of α-KG, not massive accumulation of D2-HG. Using genetic models of physiologic increment or down-regulation of D2HGDH we show that subtle modulation of D2HGDH significantly influences histone and DNA methylation, and HIF1α hydroxylation. These effects are dependent on α-KG, and can be mimicked with a synthetic cell-permeable α-KG or abrogated with its competitive inhibitor DMOG. Importantly, we show that D2HGDH meaningfully contribute to the cellular pool of α-KG by regulating IDH activity in the mitochondria, but not in the cytosol, in association with transcription induction of IDH2. Accordingly, genetic modulation of mitochondrial IDH2 rescues the effects of D2HGDH on histone and DNA methylation, and HIF1α hydroxylation. Together, these findings link D2HGDH to epigenetic remodelling in DLBCL and indicate that this enzyme is not simply a guardian against the accumulation of toxic D2-HG. Instead, our data suggest that by regulating IDH2, D2HGDH is an important player in the generation of α-KG, a metabolite that coordinates epigenetic plasticity in various model systems and influences malignant behaviour, longevity and stem cell maintenance[22,23].

Results

DLBCL-associated D2HGDH mutations

Considering the important role of α-KG in regulating the activity of dioxygenases, we sought to identify α-KG-dependent models for deregulation of epigenetic modifiers that are relevant to DLBCL biology. We centred our investigation on the genes encoding the enzymes that convert 2-HG into α-KG[9], *D2HGDH* and *L2HGDH*. We sequenced the entire coding region and intron/exon boundaries of *D2HGDH* and *L2HGDH* in an initial cohort of

69 DLBCLs and found six samples (8.7%) with four unique heterozygous mutations in *D2HGDH* (3 missense, 1 truncating), but none in *L2HGDH*. To expand on this observation, we sequenced *D2HGDH* in an additional 80 DLBCL samples, and found another missense mutation in two independent tumors. In all, 5 unique variants (four missense and one truncating deletion) were found in 8 of 149 samples (5.3%), including 4/120 primary tumours and 4/29 DLBCL cell lines (Figure 1a and Supplementary Table 1). In all instances, the mutations were heterozygous, and the mutant and wild-type alleles were equally expressed (Supplementary Figure 1). The *IDH1/2* exons that encode the 2HG-producing mutations (G97, Y100 and R132, IDH1; R140 and R172, IDH2)[24] were also sequenced in all *D2HGDH*-mutant tumours, alongside 74 other DLBCL cases, and were found to be in the wild-type (WT) configuration. We confirmed the somatic nature of the *D2HGDH* mutations in two primary tumours, but did not have constitutive DNA to examine the other cases. All *D2HGDH* mutations found in DLBCL target conserved residues and cluster either at the point of D2HGDH contact with its co-factor, FAD, or in the less well-characterized C-terminal region, a distribution similar to that found in patients with D-2-HGA (Figure 1b–c)[25]. The molecular basis of this hereditary syndrome also includes small deletions at the *D2HGDH* locus. Therefore, we used multiplex ligation-dependent probe amplification (MLPA) and real-time quantitative PCR to examine the copy number integrity of this gene in our cohort, but found no evidence for small intragenic deletion of *D2HGDH* in DLBCL (Supplementary Table 2). None of the DLBCL-associated *D2HGDH* variants that we found were present in approximately 300 normal alleles sequenced in our laboratory. However, the Exome Aggregation Consortium – EXAC database, which includes both normal and disease alleles from over 61,000 individuals, lists two of the variants that we identified (A426T and R421H) as rare SNPs (allele frequencies of 0.01% and 0.00022%, respectively). These variants were found at a much higher frequency (2.8% and 0.67%, respectively) in our cohort (Supplementary Table 1) and, as we show below, they are functionally impaired. In addition, one of these two variants, A426T, has been previously reported as the genetic basis of a family of D-2-HGA[25].

D2HGDH is a FAD-dependent mitochondrial enzyme[8], but little else is known about its functional requirements. Thus, to explore the possibility that D2HGDH forms homo-complexes, a feature common to metabolic mitochondrial enzymes, and to explore the possibility that the DLBCL-associated mutations could alter this functional requirement, we generated D2HGDH WT and mutant constructs tagged with either FLAG or HA. Co-transfection of differently tagged D2HGDH WT-WT pairs, followed by bidirectional immunoprecipitation (IP) unveiled a hitherto unreported feature of this protein, its ability to form homodimers and/or multimers (Supplementary Figure 2). However, co-transfection and IP examinations of mutant D2HGDH proteins demonstrated that these variants did not change the ability of D2HGDH to self-complex. We also examined if the DLBCL-associated mutations changed the subcellular localization of D2HGDH. Using immunofluorescence, we confirmed that D2HGDH localizes to the mitochondria and demonstrated that the mutant enzymes do not display a distinct subcellular localization (Supplementary Figure 3).

D2HGDH mutations are loss-of-function

To determine whether the five DLBCL-associated D2HGDH variants that we discovered affected the conversion of D2-HG into α-KG, we generated HEK-293 cells stably expressing the WT and mutant enzymes and used liquid chromatography-mass spectrometry (LC-MS) to quantify these metabolites. Cells expressing WT D2HGDH displayed significantly elevated α-KG levels, while cells expressing the G131X, A208T, R212W, R421H or A426T mutant constructs were indistinguishable from the isogenic empty vector control ($p<0.0001$, ANOVA) (Figure 2a and Supplementary Figure 4). In agreement with these data, the levels of D2-HG were significantly lower in cells expressing the WT enzyme than those with empty MSCV or the D2HGDH mutants G131X, A208T and R212W ($p<0.0001$, ANOVA). Surprisingly, despite the inability to effectively generate α-KG, the levels of D2-HG in cells expressing the R421H or A426T mutants were similar to those of the D2HGDH-WT counterparts (Figure 2a, Supplementary Figure 4); the reason for this discrepancy remains unclear. Importantly, as expected, ectopic expression of WT or mutant D2HGDH did not alter L2-HG levels (Supplementary Figure 4), further suggesting that metabolism of the 2-HG enantiomers is not tightly linked.

We next explored the consequences of this metabolic disruption towards α-KG-dependent dioxygenases. To that end, and to avoid the potentially confounding effect of stable overexpression models, we transiently expressed increasing (physiologic) amounts of WT and mutant D2HGDH (Figure 2b and Supplementary Figure 5). Examining these models, we found that WT D2HGDH, but none of the mutants, induced a “dose-dependent” decrease in histone H3 lysine (H3K) methylation, an increase in HIF-1α hydroxylation at proline 402 (with corresponding decrease in total HIF1α levels), and a significant increase in the abundance of 5hmC (5-hydroxy-methyl-cytosine) marks, with corresponding decrease in global 5-methyl-cytosine (5mC) levels (Figures 2b–c).These data confirm that the DLBCL-associated mutants encode an inert enzyme We attributed the cellular effects of WT D2HGDH to a heightened activity of α-KG-dependent histone demethylases (HDMs), TET enzymes and HIF1α prolyl-hydroxylases (PHDs), a consequence of the higher levels of α-KG in these cells. Indeed, we were able to confirm that the subtle increase in WT D2HGDH expression noted in this model resulted in a progressive increase and decrease of α-KG and D2-HG levels, respectively (Figure 2d and Supplementary Figure 6). Finally, as expected, the distinction between WT and mutant D2HGDH towards histone/DNA methylation and HIF1 hydroxylation was also observed in the models of stable expression (Supplementary Figure 7). Of note, recent data generated in the context of IDH1/2 mutant cell lines confirmed the ability of D2HGDH to increases α-KG and to modulate the activity of a subset of α-KG-dependent dioxygenases[26].

To confirm the role of α-KG in our system, we used the cell-permeable octyl-α-KG and fully recapitulated the effects of D2HGDH-WT expression towards histone/DNA methylation and HIF1α hydroxylation (Figure 3a–c). Consistent with these data, exposure to dimethyloxalylglycine (DMOG) abrogated the cellular effects of WT D2HGDH (Figure 3d–f), probably via competitive inhibiting of α-KG, as suggested earlier in IDH1/2 mutant models[27]. We concluded that the D2HGDH mutants encode an inactive protein, and that subtle variations on the expression the WT enzyme increases α-KG production, and thus

influence histone and DNA methylation and HIF1α hydroxylation in a manner that is compatible with higher activity of α-KG dependent dioxygenases.

D2HGDH haploinsufficiency in lymphoma

As the D2HGDH variants identified are heterozygous, and a dominant negative effect is not obvious [compare the nearly indistinguishable measurements of empty- vector vs. mutant-expressing isogenic cells in multiple assays, (Figure 2 and Supplementary Figures 4 and 7)], we used an siRNA strategy to partially knockdown WT D2HGDH in two B cell lymphoma cell lines and hence determine if a hemizygous loss of D2HGDH would be of consequence. In these assays, reducing D2HGDH protein expression by approximately half promptly increased histone methylation, decreased HIF1α hydroxylation and significantly elevated or reduced the abundance of 5hmC and 5mC DNA marks, respectively (Figure 4a–c). We expanded these observations to an HEK-293 model, and showed that transient or stable KD of D2HGDH modified the readout of function of multiple α-KG dependent dioxygenases, in association with a decrease and increase in α-KG and D2-HG levels, respectively, while again no changes were found in L2-HG levels (Supplementary Figure 8). We concluded that partial loss of D2HGDH has metabolic and cellular consequences, supporting a haploinsufficiency model for tumours with heterozygous inactivating mutation of this gene.

D2HGDH induces mitochondrial IDH activity

D2-HG is a low-abundance metabolite. Therefore, it was necessary to determine whether D2HGDH's contribution to the cellular pool of α-KG derived exclusively from the oxidation of D2-HG, or if a larger metabolic adaptation was present to explain its ability to meaningfully influence the cellular concentrations of α-KG.

First, we traced the intermediary metabolism with [U-^{13C}]glutamine in models of stable D2HGDH-WT and mutant expression, as well as of transient siRNA-mediated KD. The resulting labelling patterns did not reveal any major changes in the way that glutamine carbon is distributed into pools of metabolites along the glutamine degradation pathway, including glutamate, αKG, and other TCA cycle metabolites. Specifically, carbon from glutamine was transferred through the glutamate and α-KG pools into the TCA cycle such that there was no difference in the fractional contribution of glutamine to these metabolites in cells expressing WT or mutant D2HGDH. Nonetheless, in these same samples we confirmed the higher abundance of α-KG in cells expressing D2HGDH WT when compared to the empty-vector or mutant enzyme-expressing cells (Supplementary Table 3).

Since IDH is a major contributor to the cellular pools of α-KG, we next considered the possibility that D2HGDH may influence IDH activity. To address this possibility, IDH activity was determined by measuring the increase of absorbance at 340nm generated by the conversion of NADP to NADPH, in the presence of increasing concentrations of isocitrate; in these experiments, controls included assay solution lacking isocitrate or reactions performed in absence of protein lysate. These assays were initially performed in whole cell lysates, thus reflecting the combined IDH1 and IDH2 activities. These analyses revealed a consistent effect of D2HGDH on IDH function - cells expressing WT D2HGDH displayed higher IDH activity than those expressing an empty vector or any of the mutant enzymes,

while KD of D2HGDH markedly suppressed IDH activity (Figure 5a–b, and Supplementary Tables 4 and 5). To better characterize this observation, we isolated cytosolic and mitochondrial fractions and repeated the IDH activity assays. D2HGDH expression influenced IDH activity exclusively in the mitochondria, presumably reflecting IDH2 function (Figure 5a–b Supplementary Tables 4 and 6). We also showed that the influence of WT D2HGDH on IDH activity was "dose-dependent" and readily detected in our model of transient physiologic increase in D2HGDH expression, or partial KD of D2HGDH in B lymphoma cell lines (Supplementary Figure 9, Supplementary Tables 5 and 6).

We then considered that if these enzymatic assays were capturing a relevant cellular event, then the NADP/NAPDH ratio and consequently ROS abundance may also be modified by D2HGDH expression and mutational status. In agreement with this concept, we found a significantly lower NADP/NADPH ratio in cells expressing D2HGDH WT compared to their isogenic counterparts expressing the mutant enzyme (Figure 5c); no significant changes in NAD/NADH ratio was noted (not shown), thus possibly excluding an effect of D2HGDH towards mitochondrial IDH3. These findings were confirmed upon transient expression of physiologic levels of WT D2HGDH, whereas KD of D2HGDH in multiple cell models resulted in a higher NADP/NAPDH ratio (Figure 5c). Accordingly, cells expressing mutant D2HGDH or with a specific KD of this gene, showed significantly higher ROS levels than their isogenic counterparts expressing the WT enzyme or a siRNA control (Figure 5d). We concluded that D2HGDH modulates the cellular pool of α-KG at least in part by influencing IDH activity in the mitochondria, and we suggest that the accumulation of ROS may be part of the pathogenesis of disorders associated with D2HGDH loss.

IDH2 rescues the cellular effects of D2HGDH

We next explored how D2HGDH may influence IDH activity. To be certain that the cytosolic and mitochondrial fractions shown above were reflecting IDH1 and IDH2 function, respectively, we used western blot to detect these proteins in their subcellular compartments. Indeed, IDH1 was found exclusively in the cytosol and IDH2 in the mitochondria (Figure 6a). Remarkably, these assays also revealed that D2HGDH KD cells expressed lower IDH2 levels, while cells ectopically expressing D2HGDH had increased IDH2 abundance; D2HGDH did not influence IDH1 expression (Figure 6a). We confirmed these observations in multiple cell models, including the detection of a progressive upregulation of IDH2 upon transient expression of increasing amounts of D2HGDH (Supplementary Figure 10). Further, we found that the D2HGDH-dependent IDH2 modulation occurs at transcriptional level (Supplementary Figure 10). Next, we attempted to determine if the α-KG generated by the D2HGDH-mediated oxidation of D2-HG in the mitochondria could be involved in the regulation of IDH2 expression. To that end, we used the cell-permeable octyl-α-KG and after brief exposure (6h) we measured its effects on IDH expression. Remarkably, this synthetic α-KG readily induced IDH2, but not IDH1, at both mRNA and protein levels (Supplementary Figure 10), thus preliminarily suggesting a mechanism by which D2HGDH regulates IDH2 expression.

Lastly, we postulated that if the disruption of IDH2 expression/activity accounted for the D2HGDH-associated effects on α-KG-dependent dioxygenases, then we should be able to

"rescue" these cells with genetic modulation of IDH2 expression. To address this possibility, we created a series of dual genetic models: we stably knocked-down IDH2 in cells expressing WT D2HGDH, and we ectopically expressed IDH2 in cells with D2HGDH KD. In all models, we then quantified histone methylation, 5hmC and 5mC abundance and HIF1α hydroxylation. IDH2 knockdown fully countered the effects of WT D2HGDH, with minimal influence on MSCV control cells, whereas ectopic expression of IDH2 abrogated the effects associated with D2HGDH loss (Figure 6b–e). Importantly, modulation of IDH2 levels did not change D2HGDH expression (Supplementary Figure 11). We concluded that in our models deregulated IDH2 expression mediates at least part of the D2HGDH effects towards α-KG-dependent dioxygenases.

D2HGDH status influences the epigenetic remodelling of DLBCL

Mutations in chromatin modifying enzymes are frequent in DLBCL[21], suggesting that aberrant epigenetic remodelling is an integral component of lymphoma biology. Our data indicate that loss of D2HGDH, by disrupting the activity of α-KG-dependent dioxygenases, may also contribute to these pathogenic epigenetic changes. To address this possibility, we first investigated a panel of parental DLBCL cell lines and primary tumours expressing either mutant or WT D2HGDH. We consistently found that the D2HGDH-mutant DLBCL cell lines (n=4) displayed higher H3K methylation, lower HIF1α hydroxylation, lower levels of 5hmC and more prominent DNA methylation (Figure 7a–b) than their WT counterparts (n=10). D2HGDH-mutant primary DLBCLs also displayed higher H3K methylation, fewer 5hmC marks and higher global DNA methylation than the D2HGDH-WT biopsies (Figure 7c–d). Importantly, although some of the DLBCL cell lines and primary tumours examined harbour mutations in histone methylation regulators (Supplementary Tables 7 and 8), the presence of these abnormalities, appears to not influence the D2HGDH-driven separation in groups of samples with high and low H3K4/K9 methylation levels. To better understand how the D2HGDH status may be driving this dichotomy, we performed three independent LC-MS-based measurements of α-KG and D2-HG levels in DLBCL cell lines mutant or WT for D2HGDH. Although the abundance of these metabolites varied greatly across these samples, when taken as a group we found lower levels of α-KG (but not higher levels of D2-HG) in D2HGDH-mutant compared to WT samples; this observation correlated well with a trend for lower expression of IDH2 in D2HGDH mutant DLBCL cell lines (Supplementary Figure 12).

To further isolate the role of D2HGDH in these processes, we generated another genetic model by ectopically expressing WT-D2HGDH in each of the four D2HGDH mutant cell lines, and measured its consequences on DNA and histone methylation as well as HIF1α-hyroxylation. Expression of the WT enzyme in these mutant cells readily modified H3K methylation, HIF1α hydroxylation, and the abundance of 5hmC marks. In agreement with a role for α-KG in this process, these D2HGDH-induced cellular effects were fully reversed by DMOG (Supplementary Figure 13). Notably, ectopic expression of WT D2HGDH in the mutant DLBCL cell lines also induced IDH2 expression, further linking the activity of these two mitochondrial proteins (Supplementary Figure 13). We concluded that as a group, DLBCL harbouring mutant D2HGDH display lower α-KG levels, a trend for lower IDH2 expression, which we suggest accounts for the broad deregulation of dioxygenases.

Discussion

In this work, we report discoveries with implications to the fields of cancer, metabolism and epigenetic remodelling. We identified and functionally characterized D2HGDH mutations in DLBCL and elucidated a previously unknown mitochondrial cross-talk between D2HGDH and IDH2. These findings point to α-KG as an important metabolite in regulating the plasticity of the epigenome.

The discovery of *D2HGDH* mutations in DLBCL is of relevance because mutation in epigenetic modifiers has recently been shown to be one of the hallmarks of this malignancy[21]. Certainly, the frequency of D2HGDH mutations in DLBCL that we are reporting is low. However, recent evidence suggest that the discovery of cancer genes has not yet reached saturation, and that larger sample sizes will be needed to identify the true mutation frequencies of less frequently targeted sequences[28]. In agreement with this argument, D2HGDH variants were not reported following systematic screens of the DLBCL exome[15–18], possibly reflecting the sample size and frequency threshold for mutation calls used in those studies (Supplementary Note). Our data indicate that *D2HGDH* is one of genes that when mutant may promote epigenetic reprograming in DLBCL. Demonstration that D2HGDH-mutant DLBCL cell lines display lower α-KG levels, and that this metabolite markedly influence histone and DNA methylation is consistent withthis concept. However, we acknowledge that given the heterogeneity of DLBCL, one cannot exclude the possibility that additional genetic events may contribute to part of the epigenetic differences that we found in the DLBCL cell lines and primary tumours dichotomized by the D2HGDH status. Nonetheless, the role of D2HGDH in driving at least part of this remodelling is supported by multiple isogenic B cell lymphoma models of loss and gain of D2HGDH function.

Although loss-of-function mutations in *D2HGDH* have long been shown to cause type I D-2-hydroxyglutaric aciduria[25], ours is the first detailed report of mutation of this mitochondrial enzyme in cancer. Nonetheless, upon reviewing recent systematic genetic screens of various solid tumours and in the related Burkitt lymphoma[29] we noted the presence of rare somatic D2HGDH mutations with similar features of those that we found in DLBCL, including: targeting of highly conserved residues, primarily missense changes, heterozygous status, clustering in two protein regions and, on occasion, previous description in families with type I D-2-hydroxyglutaric aciduria (Supplementary Table 9). We conclude that rare somatic D2HGDH mutation is a pervasive event in cancer; as mutation frequency is not an absolute determining factor for their relevance[28], we propose that the final determination as to whether D2HGDH variants contribute to cancer initiation and/or progression awaits the generation of relevant mouse models. Finally, it is important to make a distinction between the reported higher risk of cancer in patients with deficiency of L2HGDH[13], and the apparent lack of such effects in infants diagnosed with D-2-HGA. Here, it should be noted that D-2-HGA may have a more aggressive clinical course than L-2-HGA[11,25], and as the patients succumb to their disease more rapidly, it may not be possible to determine whether deficiency of D2HGDH can also influence the long-term susceptibility to cancer.

The D2HGDH mutations described in type I D-2-hydroxyglutaric aciduria and in DLBCL are highly clustered. Using structural modelling, we showed that one group of mutants locates close to the point of contact with the enzyme's co-factor FAD. Disruption of these interactions is likely to affect the enzyme's activity and can be easily reconciled with a loss-of-unction phenotype. The second cluster of mutations mapping the c-terminus of the protein is more intriguing. This region does not possess are recognizable structural or functional domain, and yet its consistent disruption in D2HGDH-related conditions suggest that it is important for the enzyme's activity. We explored the possibility that this region could be a putative dimerization or subcellular localization domain. While we discovered that D2HGDH can homodimerize, none of the mutations affected this property nor did they change the enzymes' mitochondrial localization. Complete characterization of the functional domains of D2HGDH is an important future objective.

D2-HG is considered an unwanted byproduct of cellular metabolism with no known physiologic role[9]. It is certain nonetheless that cellular accumulation of D2-HG is toxic, as evidenced by the extensive neurologic disease and rapid clinical deterioration of infants with bi-allelic loss of D2HGDH. The enzymatic activity of D2HGDH helps keep the intracellular levels of D2-HG below <0.1 mM and to date this has been considered the primary, if not only, function of this dehydrogenase[9]. However, our data suggest otherwise. We have shown that even modest increases in D2HGDH expression markedly elevated the levels of intracellular α-KG. This observation was at first puzzling for it was unclear how the D2HGDH-dependent interconversion of the nearly undetectable D2-HG into α-KG, could contribute significantly to the mM cellular concentrations of α-KG. We solved this conundrum with an enzymatic examination of IDH activity in sub-cellular fractions and the demonstration that D2HGDH positively influences the expression and activity of the mitochrondrial IDH2, but not the cytosolic IDH1. Together, these observations challenge the notion that D2HGDH is simply a cellular guardian against the toxic accumulation of D2-HG. Instead, our data suggest that D2HGDH may function a rheostat dialling up and down IDH2 function and, therefore, the intracellular levels of α-KG. We also made inroads in the initial characterization on the mechanism by which D2HGDH positively influences IDH2 expression. We showed that a synthetic cell permeable α-KG recapitulates the effects of D2HGDH and also induce IDH2 transcription. It still remains to be determined if α-KG acts directly on the IDH2 promoter or if it uses intermediates – the rapid (6h) effects of synthetic α-KG suggests that in this context IDH2 behaves as an immediate early gene and it is transcriptionally induced before any new proteins are synthesized. These data also demonstrate an important difference in the regulation of the related IDH1 and IDH2 proteins. Together, these observations led us to speculate that physiologically, the local (mitochondrial) increment in α-KG levels resulting from the D2HGDH-driven conversion of D2-HG into α-KG induces IDH2 transcription. Important tasks for future studies include characterization of the elements in the IDH2 promoter, and associated transcription factors, that may mediate this response. In addition, the demonstration that discrete increments in D2HGDH levels influence α-KG abundance and the activity of multiple epigenetic modifiers, make the that identification of the signals and regulatory elements that drive D2HGDH expression a high priority for additional investigations.

One notable distinction between our data and those derived from somatic gain-of-function IDH1/2 mutation, or bi-allelic loss of D2HGDH in the germline, is that the principal metabolic consequence of the heterozygous D2HGDH mutations found in DLBCL is deficiency of α-KG, not massive accumulation of D2-HG. It can speculated that considering the very low intracellular levels D2-HG even when D2HGDH is functioning at half capacity (i.e. heterozygous loss) it still can prevent D2-HG accumulation. However, because D2HGDH uses IDH2 to modify the total pool of intracellular α-KG, we suggest that the modest mitochondrial change in α-KG abundance derived from a haploinsufficient D2HGDH can have large repercussions. Irrespective of the precise underpinnings, our data suggest that subtle D2HGDH-mediated changes in α-KG levels may regulate the activity of dioxygenases and rewrite several epigenetic marks. Indeed, we show that discrete changes in D2HGDH levels or a brief exposure to synthetic α-KG or its competitive inhibitor DMOG influence histone and DNA methylation, as well as HIF1α hydroxylation. These data bring to the fore the relevance of α-KG in multiple cellular functions, as recently highlighted in a nematode model and in embryonic stem cells[22,23]. We propose that once better understood at molecular and cellular levels, modulation of α-KG with therapeutic intent may have a role in cancer therapeutics.

In conclusion, by characterizing rare D2HGDH mutations found in DLBCL, we unveiled an unsuspected role for this enzyme in modulating IDH2 expression and activity, and consequently the cellular α-KG pool. In our models, subtle titration of D2HGDH levels had a marked repercussion towards histone and DNA methylation and HIF1α hydroxylation, consistent with a change in the activity of α-KG-dependent dioxygenases. Our findings also indicate that the relevance of D2HGDH to cellular physiology may extend beyond preventing the toxic accumulation of D2-HG, and underscore the need for a tight control of D2HGDH expression since modest variations of its levels can engage an IDH2-α-KG-dioxygenases axis that has the potential for profound effects on cellular regulation including by epigenetic remodeling. Strikingly, the finding of IDH2 (but not IDH1) gain of function mutations in type II D-2-HGA patients[30] provides an independent validation of the hitherto unsuspected biological connectedness between D2HGDH and IDH2. Finally, our data may advance the understanding of hereditary conditions that associate with D2HGDH dysfunction.

Methods

Primary DLBCL samples and cell lines

Frozen biopsies from 72 untreated DLBCL patients were obtained from our local tumor bank, Department of Pathology, University of Texas Health Science Center at San Antonio. The clinical, pathological, and molecular features of this tumor collection were described previously[31]. Tissue was available from an additional 48 DLBCL cases diagnosed at the Division of Hematology, Medical University of Graz, Austria. Protein was also isolated from twelve primary DLBCLs (4 D2HGDH-mutant and 8 D2HGDH-WT); the selection of the D2HGDH-WT or mutant for further analyses was based on the availability of frozen material and their clinical/phenotypical similarities. The use of these samples was approved by the Review Boards of each Institution. The DLBCL cell lines SU-DHL2, SU-DHL4, SU-

DHL6, SU-DHL8, SU-DHL10, OCI-Ly1, OCI-Ly4, OCI-Ly7, OCI-Ly8, OCI-Ly10, OCI-Ly18, OCI-Ly19, Farage and WSU-NHL were cultured at 37°C in 5% CO2 in RPMI-1640 medium (Invitrogen) containing 10% (vol/vol) FBS (or 20% FBS for SU-DHL2 and OCI-Ly10 cultures), while HEK-293 cells were maintained in Dulbecco's modified Eagle media (DMEM; Mediatech) with 10% FBS, as we described[32]. All D2HGDH-mutant DLBCL cell lines are of the GCB molecular subtype, thus we initially selected five D2HGDH-WT cell lines also of the GCB subtype (SU-DHL4, SU-DHL10, OCI-Ly1, OCI-Ly4, OCI-Ly18) for comparison[15]. This group was next extended to include five additional D2HGDH-WT DLBCL cell lines (SU-DHL2, Farage, OCI-Ly8, OCI-Ly10, OCI-Ly19) also characterized by WT configuration of multiple chromatin modifier genes (MLL2, MLL3, MLL4, MLL5 and EZH2; Supplementary Table 7) that are relevant in the present context. The identity of the mutant DLBCL cell lines was confirmed by VNTR analysis and verified online at the DSMZ cell bank (http://www.dsmz.de) and tested for Mycoplasma contamination before this project started. All cell lines were pre-existent in our group, and were earlier obtained from ATCC or DSMZ cell bank or from Margaret Shipp (OCI-Ly10) (Dana-Farber Cancer Institute), Laura Pasqualucci (SU-DHL2) (Columbia University) or Sandeep Dave (HBL-1, U2932) (Duke University).

DNA isolation and sequencing

High molecular weight DNA from the primary DLBCL biopsies (n=120) and DLBCL cell lines (n=29) was isolated using Gentra Puregene DNA purification kits (Qiagen). For all 149 samples, the nine coding exons (and exon/intron junctions) of D2HGDH were amplified; the 10 coding exons (and exon/intron junctions) of the L2HGDH gene were PCR amplified from 68 samples; the exon 4 of IDH1 and IDH2 were amplified in 80 samples (primers sequence in Supplementary Table 10). The resulting 2,172 amplicons were sequenced directly from both strands, and compared to the reference germline sequences, using the Mutation Surveyor Version 2.41 (Softgenetics), as we described[33]. All variants were verified at the human dbSNP Database (Build 132) and Ensembl Database. All mutations were confirmed on independent PCR products, and the somatic nature of the mutation was documented in two cases with matched normal DNA (bone marrow) available. The identity of the mutant DLBCL cell lines was confirmed by VNTR analysis and verified online at the DSMZ cell bank (http://www.dsmz.de). The exons 4, 5, 8 of D2HGDH were also PCR amplified and sequenced in 190 control alleles and exon 9 in 290. For the mutant samples with available RNA (cell lines WSU-NHL, SU-DHL6 and SU-DHL8, and primary biopsy #6902), RT-PCR was used to amplify a fragment spanning multiple exons and encompassing the variant nucleotide. Subsequent sequencing (or cloning followed by sequencing) of these fragments was implemented for quantification of the relative contribution of the mutant and WT alleles to D2HGDH expression.

Copy number analysis within the D2HGDH locus

To detect copy-number variations within the D2HGDH gene we used multiplex ligation-dependent probe amplification (MLPA) and real-time semi-quantitative PCR (Q-PCR). Exons 2, 6, 7, 9 and 10 were analysed with the SALSA P107 MLPA kit (MRC-Holland), according to manufacturer's instructions. The copy-number of exons 3, 4, 5, 8 and of a region 4 Mbp upstream to the gene's transcription start site was determined by relative

quantification using Q-PCR. Tumour samples (n= 50, Supplementary Table 2) were compared to a commercially available control DNA (Promega, Madison) and normalized by a control PCR product on chromosome 22. Relative abundance (copy-number variation) was determined by the $2^{-\Delta\Delta CT}$ method[31].

Structure prediction

Sequence alignment of D2HGDH amino acid sequence against the NCBI database identified D2HGDH as containing a conserved FAD binding domain. Subsequent searches of the structural database (RSCB Protein Data Bank, Release Jan 10, 2013) using the protein threading algorithm HHPRED[34] identified a number of flavoproteins with E (expect) values of 10^{-40} or lower, and in turn near 100% probability that these are representative of the overall fold of human D2HGDH. The best scoring structure, a putative dehydrogenase from Rhodopseudomonas palustris (PDB code 3pm9, Joint Center for Structural Genomics, unpublished), had an E-value of 3.2×10^{-80}. To provide a structure-based explanation for the DLBCL-associated mutations, as well as the mutations previously reported in patients with D-2-hydroxyglutaric aciduria[25], a homology model for D2HGDH was generated using the program SwissModel[35] with chain A from 3pm9 as the template structure and the amino acid alignment derived from the HHPRED analysis above. The structures shown in Figure 1c were generated using the program UCSF Chimera[36]

Generation of genetic D2HGDH models

A sequence-verified WT D2HGDH cDNA encompassing its complete coding region was cloned into the MSCV-eGFP vector. Site-direct mutagenesis was introduced by PCR, and all mutants sequence verified. Retrovirus production and transduction in HEK-293, SU-DHL6, SU-DHL8, WSU-NHL, and OCI-Ly7 cells was performed as we described[37] and enriched GFP-positive populations (> 90% purity) obtained by Fluorescence Activated Cell Sorting (FACS). Stable ectopic expression of D2HGDH was confirmed by western blot and real-time RT-PCR. Electroporation or lipid-based transfections of the same constructs were used to generate models of transient expression of increasing (physiologic) amounts of D2HGDH (WT or mutant) in HEK-293 cells.

RNAi-based D2HGDH suppression

Transient KD of *D2HGDH* (siRNA) in HEK-293, Ly8 and RAMOS cell lines (WT for the *D2HGDH* gene) was achieved by lipid-based transfection of two independent oligonucleotides specific to this gene; these same sequences were also cloned into the pSilencer vector, as we described[38], and stable D2HGDH shRNA cells established by puromycin selection. Efficacy of the knockdown was determined by western blot.

Molecular biology and homodimerization assays

A WT D2HGDH cDNA was PCR-amplified and sub-cloned in-frame with HA (N-terminus, pHM6 plasmid) or FLAG (C-terminus, p3xFLAG-CMV plasmid) tags. The missense D2HGDH mutants (A208T, R212W, R421H and A426T) were PCR-amplified and cloned in-frame with FLAG at the C-terminus, whereas the truncating G131X mutant was fused to an N-terminus HA tag. All constructs were sequence verified. Subsequently, pairs of HA

and FLAG-tagged D2HGDH constructs (HA-WT + WT-FLAG; HA-G131X + WT-FLAG; HA-WT + A208T-FLAG; HA-WT + R212W-FLAG; HA-WT + R421H-FLAG; HA-WT + A426T-FLAG) were co-transfected in HEK-293 cells, harvested at 48h post-transfection, immunoprecipitated (IP) overnight at 4°C with anti-FLAG antibody (mouse monoclonal M2, Sigma) or anti-HA antibody (goat polyclonal, Bethyl Laboratories), and analysed with immunoblots for the pull-down HA-D2HGDH and D2HGDH-FLAG, respectively. Controls included the co-transfections with empty HA or FLAG vectors, and IPs with mouse Ig and goat serum. Equal expression of HA and FLAG fusions in the input protein was determined by western blotting. The expression of the D2HGDH fusion proteins was also determined in non-denaturing conditions. In those assays, the protein lysates of the multiple co-transfection indicated above, were subjected to electrophoresis with classical denaturing protocol side-by-side with a non-denaturing setting (sample buffer lacking SDS and 2-mercaptoethanol), and immunoblotted with anti-FLAG (1:2000), anti-HA (1:1000)and anti-D2HGDH (1:1000) antibodies.

D2HGDH and IDH2 ectopic expression and knockdown

To generate the IDH2 construct, the gene's complete coding sequence was PCR amplified from a pOTB7-IDH2 clone (IMAGE:2959540, Invitrogen), sequence verified and sub-cloned into MSCV. Next, HEK-293 cells stably expressing two shRNA constructs directed at D2HGDH (sh#3 and sh#5) or a sh-ctrl vector, were transduced with empty MSCV or MSCV-IDH2 viruses, and highly purified cell populations obtained by cell sorting. Two previously described shRNA pLKO.1-puromycin constructs directed at IDH2[39], or shRNA-pLKO.1 control were transduced into HEK-293 cells expressing and empty MSCV-vector or MSCV-D2HGDH, and stable IDH2 KD populations obtained with puromycin selection. In various models, IDH2 expression was also determined at mRNA level using real-time RT-PCR.

Protein isolation and western blots

For all experiments, cell lines were grown overnight in 5% FBS media before protein isolation, carried out in 2% SDS, 4% Glycerol, 0.04M Tris-HCL pH= 6.8 and 2mM 2-mercaptoethanol. For HIF1α (hydroxylation and total levels) analysis, cells were grown for 16h in 1% O2 in a hypoxia chamber (Invivo2 200, Ruskinn), and protein harvested inside the chamber. In other assays, a 6-h exposure to 1mM dimethyloxalylglycine (DMOG; Frontier Scientific) or to 0.5mM and 1mM of octyl-α-KG (Cayman Chemical) was carried out before protein isolation. Proteins were detected with specific antibodies directed at: D2HGDH (Proteintech, #13895-1-AP), H3K4me3, H3K9me2, H3K27me3, H3K36me3, H3K79me2 and histone H3 (all from Cell Signaling Technology), HIF1α (BD Biosciences, #61095), HIF1α-hydroxyproline (Pro402)(Millipore, #07-1585), GLUT1 (Novus Biologicals, # NB300-666), IDH1 (Cell Signaling Technology, #8137), IDH2 (Abcam, #ab55271), β-actin (Sigma-Aldrich, #A2228). For examination of GLUT1, the samples were not heat-denatured before gel loading. All PVDF membranes were stripped with OneMinute Western Blot Stripping Buffer (GM Biosciences, #GM6001) and re-probed with histone H3 and β-actin antibodies for loading control. Supportive information on the antibodies utilized is detailed on Supplementary Table 11 All antibodies were used at 1:1000 dilution, except for and β-actin (1:20000). See uncropped western blots in Supplementary Figure 14.

IDH Activity Assay

The activity of isocitrate dehydrogenase was determined by measuring the increase of absorbance at 340nm generated by the conversion of NADP to NADPH at 25°C. These assays were performed in total cell lysate, as well as in cytosol and mitochondrial fractions. The standard assay solution (1ml) contained 2mM MnCl2, 0.25mM NADP+, and DL-isocitrate concentrations ranging from 0.5 to 100μM (DL-Isocitric acid, trisodium sate hydrate, 95%, ACROS), as described[40]. Controls included assay solution lacking isocitrate or reactions performed in absence of protein lysate (in both cases yielding no measurable enzymatic activity). All experiments were performed in triplicate. NADPH production was calculated using the NADPH extinction coefficient of 6.22 mM−1 cm−1. The kinetic parameters (Km and Vmax values) were generated by a plot of enzymatic activities versus substrate concentrations, and calculated by the Graph-Pad Prizm Software using the Michaelis-Menten equation.

Mitochondria Fractionation

To separate mitochondria from cytosol, HEK-293 cells were resuspended in lysis buffer containing 200 mM manitol, 68 mM sucrose, 10 mM HEPES-KOH pH 7.4, 1 mM EGTA, and protease and phosphatase inhibitors. Cells were disrupted with multiple strokes of a glass douncer, followed by centrifugation and at 600 g for 10 minutes. Subsequently, the supernatant was collected and centrifuged at 7000 g for 10 minutes, yielding a pellet representing the mitochondria- enriched fraction. The supernatant (representing the cytosolic fraction) was centrifuged one time (14000 rpm for 10 minutes) to remove light membranes from the cytosol. To confirm the purity of the fractions, western blotting for SDHB (Invitrogen, #459230) (mitochondrial) and β-actin (cytosol) were performed.

Flow Cytometry-based 5hmC measurement

HEK-293 cells stably expressing D2HGDH WT or mutant were washed once with PBS, fixed in 1.5% formaldehyde, and permeabilized with 0.1% Triton X-100 in PBS for 15 minutes. Cells were then washed and resuspended in 1% BSA/PBS for 1hr. Anti-5hmC antibody (Active Motif, #39796), was added at 1:500 for 2h at room temperature (RT), followed by three washes in PBS, and incubation with a secondary antibody conjugated with PE (Invitrogen, #P2771MP) at 1:500 for 1h in the dark. Subsequently, the cells were washed three times in PBS and analysed using a Becton Dickinson LSRII. FACS data were analysed using FACSDiva Software (Becton Dickinson).

Quantitative 5hmC and 5mC assays

High-molecular weight DNA was obtained from relevant cell lines and primary tumours. For the quantification of 5hmC and 5mC marks, 200ng and 100ng of DNA, respectively, was added to each well (96-well plate format), followed by incubation with primary (anti-5hmC or anti-5Mc) and secondary antibodies and developed by colorimetric methods. Abundance of 5hmC and 5mC marks was quantified by absorbance, and reported as relative values to the positive controls, methylated polynucleotide containing 20% of 5hmC or 50% 5mC, respectively. In our study, the diametrically opposed levels of 5hmC and 5mC in the same cell model reinforce the high specificity of these measurement, and absence of cross-

reactivity between these modifications when defined by these assays. The high concordance between the 5hmC quantifications performed by the FACS or absorbance (Supplementary Figure 7), further confirm the reliability of this methodology. For the 5hmC and 5mC measurements, at least three independent replicates were performed, and when sufficient DNA was available (for the primary tumours) the assays done in triplicate.

Immunofluorescence

HEK-293 cells stably expressing WT or mutant D2HGDH were plated on poly-D-lysine-coated glass coverslips in 24-well tissue culture plates. After 24h, full-media containing 250nM of the cell-permeable Mito Tracker probe (Invitrogen, #M22426) was added, and incubated for 20 minutes. Next, the cells were rinsed in PBS and fixed in 4% paraformaldehyde for 15 minutes, followed by permeabilization and blocking with 5% horse serum, 0.2% Triton X-100 in PBS. Upon removal of the blocking solution, the primary antibody (anti-D2HGDH, Proteintech, #13895-1-AP) was added at 1:100 in 0.3% Triton X-100/PBS solution, and incubated for 1 hour at room temperature. After three washes with PBS, the Cy3-labeled secondary antibody (1:200) (Jackson ImmunoResearch,# 711-166-152) was added for 1h at room temperature in the dark, followed by three washes in PBS. Coverslips were mounted on glass slides using Vectashield (Vector Laboratories) for imaging. Images were acquired by laser scanning confocal microscope (LSCM) with Olympus FV1000 imaging system,[33]. The UPLANAPO 60x oil objective (1.42NA) was used for all analyses, and an additional electronic zoom of 3 was applied. Excitation and emission signals were respectively 488 and 500±35nm for GFP (expressed from a bicistronic construct), 534 and 560–660nm for Cy3 (D2HGDH), 644 and 665 nm for Cy5 (MitoTracker).

Metabolite extraction and quantification by LC–MS

HEK-293 cells stably or transiently expressing WT or mutant D2HGDH, HEK-293 with transient knockdown of D2HGDH, as well as 14 DLBCL cell lines (four D2HGDH mutant and 10 WT) were grown overnight in 5% FBS media, gently washed in PBS, collected and flash-frozen in dry-ice. For α-KG assays, the cells were extracted with cold 80% aqueous methanol (−80 °C) containing 0.6 nmol [1,2,3,4-$^{13}C_4$]α-ketoglutaric acid (Cambridge Isotope Laboratories) and maintained at −80 °C for 1 h, as described[41]. Subsequently, the extracts were centrifuged at 13,800 × g for 10 minutes and the supernatants were transferred to glass autosampler vials for HPLC-electrospray ionization-mass spectrometry (HPLC-ESI-MS) analysis. The processing of the samples for 2-HG analysis was as above except that 2 nmol [1,2,3,4-$^{13}C_4$]L-malic acid (Cambridge Isotope Laboratories) was added as the internal standard and the dried extracts were reacted with diacetyl-L-tartaric anhydride (Sigma-Aldrich), as described[42]. HPLC-ESI-MS analyses were conducted on a Thermo Fisher Q Exactive mass spectrometer with on-line separation by a Thermo Fisher/Dionex Ultimate 3000 HPLC. HPLC conditions for KG analyses were: column, Luna NH_2, 3 μm, 2 × 150 mm (Phenomenex); mobile phase A, 5% acetonitrile in water containing 20 mM ammonium acetate and 20 mM ammonium hydroxide, pH 9.45; mobile phase B, acetonitrile; flow rate, 300 μL/min; gradient, 85% B to 1% B over 10 minutes and held at 1% B for 10 minutes. The conditions used to separate D-HG from L-HG analyses were: column, Kinetex C18, 2.6 μm, 2.1 × 100 mm (Phenomenex); mobile phase, 1% acetonitrile with 125 mg/L ammonium

formate, pH 3.6; flow rate, 400 μL/min. For both analyses, full scan mass spectra were acquired in the orbitrap using negative ion detection over a range of *m/z* 100 – 800 at 70,000 resolution (*m/z* 300). Metabolite identification was based on the metabolite accurate mass (± 5 ppm) and agreement with the HPLC retention time of authentic standards. Quantification was made by integration of extracted ion chromatograms of each metabolite followed by comparison with the corresponding standard curves. For these analyses, α-ketoglutaric acid (KG) and D-hydroxyglutaric acid (D-HG) were obtained from Sigma-Aldrich and the HPLC-grade solvents from Fisher Scientific.

The measurements of the D2-HG, L2-HG and α-KG metabolites were also independently performed by LC-MS/MS[43,44] In brief, 20 μl aliquot of the extracted samples were injected for chromatographic separation on an Agilent Hypersil ODS 4.0 × 250 mm, 5 μm column (Santa Clara, CA). The column oven was set at 30°C. Solvent A was 125 mg/L ammonium formate, pH = 3.6, solvent B was acetonitrile. The enantiomers were eluted using the program: 0 to 0.5 min – 100% A, 0.5 to 3.5 min – linear gradient to 96.5% A, 3.5 to 25 min - 96.5% A and 3.5% B. The flow rate was set at 0.5 ml/min, 50% of the post-column eluate was diverted to waste, and the remainder injected into API 3000 triple-quadrupole mass spectrometer equipped with an electrospray ionization source (Applied Biosystems, Foster City, CA) and operating in negative ion mode. Turbo ionspray gas was set at 8 L/min, the temperature at 500°C, and the ionspray voltage at 4200 V for 2-HG and at −1700 V for 2-KG. Product ion transitions were monitored at 363.2 to 147.2 for L-2-HG and D-2-HG, 367.1 to 151.1 for D,L-[3,33,4,4-D_4]-2-hydroxyglutaric acid, 145.15 to 101.1 for α-KG, and 149.2 to 105.2 for 2-ketopentanedioic acid-[D_4]. Protein concentration was measured using the RC DC Protein Assay (Bio-Rad, Irvine, CA) and on SmartSpec Plus (Bio-Rad). All metabolite data are shown in Figure 2, Supplementary Figure 4, Supplementary Figure 6, Supplementary Figure 12 and Supplementary Table 12.

Measurement of α-KG abundance

Cells were cultured in DMEM containing [U-^{13}C]glutamine and extracts were collected in ice cold 1:1 methanol:water, subjected to three freeze-thaw cycles, and cell debris removed by high-speed centrifugation with cold 80% aqueous methanol[45]. Subsequently, the supernatant was split into two glass tubes and evaporated with blown air at 42°C. To one of the dried samples, 25 nmoles of unlabelled α-KG was added and the sample was evaporated to dryness again. To all samples, 50 μL of methoxyamine-hydrochloride in pyridine (2%) was added and the samples were left at room temperature overnight (~16h). The samples were then evaporated again and derivatized in 100 μL Tri-Sil reagent (Thermo) at 42°C for 1.5h. All samples were then injected onto an Agilent 6890N gas chromatograph networked to an Agilent 5975 Mass Selective Detector. Mass isotopomer distribution was determined for α-KG using methods analogous to those used for other TCA cycle intermediates[45]. The abundance of α-KG was calculated based on the fold dilution of enrichment caused by addition of 25 nmoles unlabeled α-KG.

Measurement of NADP/NADPH and ROS levels

NADP/NADPH levels were quantified using an assay kit from Abcam (ab65349) and performed according its instructions. In brief, multiple cell models of D2HGDH ectopic

expression or KD were extracted using the manufacturer provided buffer, mixed with NADP cycling solution, with the NADPH developer and absorbance measured at OD450nm. Total NADP and NADPH concentrations were calculated by correlation to the curve generated with the NADPH standard (NADPH DS). NAD/NADH levels were quantified as above, but using the Abcam assay kit #ab65348. For ROS detection, we performed DCFDA assays (Life Technologies/Molecular Probes #C6827). In brief, cells were incubated with 10μM of CM-H_2DCFDA (5-(and-6)-chloromethyl-2′,7′-dichlorodihydrofluorescein diacetate, acetyl ester) at 37°C for 10 min. Excess CM-H_2DCFDA was removed by washing the cells twice in PBS, followed by lysis in 10% NP40 buffer. The homogenates were centrifuged to remove cellular debris. Oxidation of DFCDA to DFC (a measure of ROS generation) was determined using a spectrofluorometer with excitation at 495 nm and emission at 525 nm.

Statistics

Analyses were performed using a one-way ANOVA, with Bonferroni's Multiple Comparison post-hoc test, and by two-tailed Student's t-test or Mann-Whitney test. Equal variance was calculated with an F test (t-test) or with a Bartlett's statistics for equal variances (ANOVA, groups with five or more values). $P < 0.05$ was considered significant. Data analyses were performed in the Prism software (version 5.02, GraphPad Software Inc) and Excel (Microsoft).

Supplementary Material

Refer to Web version on PubMed Central for supplementary material.

Acknowledgements

We thank Marsha Kinney and the Pathology Core Laboratory at the University of Texas HSC San Antonio, for procurement of the primary DLBCL samples; C. Beham-Schmid for providing bone marrow specimens; K. Lind and S. Hofer for VNTR analyses. This work was supported by an NIH grant R01-CA138747 (to R.C.T.A), a CPRIT award RP140452 (to R.C.T.A.), Young Investigator Awards from the Voelcker Fund (to P.L.M.D and R.C.T.A), Leukämiehilfe Steiermark (to H.S.), and a Cancer Center support grant P30 CA054174.

References

1. Dang L, et al. Cancer-associated IDH1 mutations produce 2-hydroxyglutarate. Nature. 2010; 465:966. [PubMed: 20559394]
2. Gross S, et al. Cancer-associated metabolite 2-hydroxyglutarate accumulates in acute myelogenous leukemia with isocitrate dehydrogenase 1 and 2 mutations. The Journal of experimental medicine. 2010; 207:339–344. [PubMed: 20142433]
3. Ward PS, et al. The common feature of leukemia-associated IDH1 and IDH2 mutations is a neomorphic enzyme activity converting alpha-ketoglutarate to 2-hydroxyglutarate. Cancer cell. 2010; 17:225–234. [PubMed: 20171147]
4. Loenarz C, Schofield CJ. Expanding chemical biology of 2-oxoglutarate oxygenases. Nature chemical biology. 2008; 4:152–156. [PubMed: 18277970]
5. Lu C, et al. IDH mutation impairs histone demethylation and results in a block to cell differentiation. Nature. 2012; 483:474–478. [PubMed: 22343901]
6. Turcan S, et al. IDH1 mutation is sufficient to establish the glioma hypermethylator phenotype. Nature. 2012; 483:479–483. [PubMed: 22343889]
7. Losman JA, et al. (R)-2-hydroxyglutarate is sufficient to promote leukemogenesis and its effects are reversible. Science. 2013; 339:1621–1625. [PubMed: 23393090]

8. Achouri Y, et al. Identification of a dehydrogenase acting on D-2-hydroxyglutarate. The Biochemical journal. 2004; 381:35–42. [PubMed: 15070399]
9. Struys EA. D-2-Hydroxyglutaric aciduria: unravelling the biochemical pathway and the genetic defect. Journal of inherited metabolic disease. 2006; 29:21–29. [PubMed: 16601864]
10. Kranendijk M, Struys EA, Salomons GS, Van der Knaap MS, Jakobs C. Progress in understanding 2-hydroxyglutaric acidurias. Journal of inherited metabolic disease. 2012; 35:571–587. [PubMed: 22391998]
11. Steenweg ME, et al. An overview of L-2-hydroxyglutarate dehydrogenase gene (L2HGDH) variants: a genotype-phenotype study. Human mutation. 2010; 31:380–390. [PubMed: 20052767]
12. Rzem R, et al. A gene encoding a putative FAD-dependent L-2-hydroxyglutarate dehydrogenase is mutated in L-2-hydroxyglutaric aciduria. Proceedings of the National Academy of Sciences of the United States of America. 2004; 101:16849–16854. [PubMed: 15548604]
13. Moroni I, et al. L-2-hydroxyglutaric aciduria and brain malignant tumors: a predisposing condition? Neurology. 2004; 62:1882–1884. [PubMed: 15159502]
14. Shim EH, et al. L-2-Hydroxyglutarate: an epigenetic modifier and putative oncometabolite in renal cancer. Cancer discovery. 2014; 4:1290–1298. [PubMed: 25182153]
15. Pasqualucci L, et al. Analysis of the coding genome of diffuse large B-cell lymphoma. Nat Genet. 2011; 43:830–837. [PubMed: 21804550]
16. Morin RD, et al. Frequent mutation of histone-modifying genes in non-Hodgkin lymphoma. Nature. 2011; 476:298–303. [PubMed: 21796119]
17. Lohr JG, et al. Discovery and prioritization of somatic mutations in diffuse large B-cell lymphoma (DLBCL) by whole-exome sequencing. Proc Natl Acad Sci U S A. 2012; 109:3879–3884. [PubMed: 22343534]
18. Zhang J, et al. Genetic heterogeneity of diffuse large B-cell lymphoma. Proc Natl Acad Sci U S A. 2013; 110:1398–1403. [PubMed: 23292937]
19. Quivoron C, et al. TET2 inactivation results in pleiotropic hematopoietic abnormalities in mouse and is a recurrent event during human lymphomagenesis. Cancer cell. 2011; 20:25–38. [PubMed: 21723201]
20. Cimmino L, et al. TET1 is a tumor suppressor of hematopoietic malignancy. Nature immunology. 2015
21. Pasqualucci L. The genetic basis of diffuse large B-cell lymphoma. Curr Opin Hematol. 2013; 20:336–344. [PubMed: 23673341]
22. Carey BW, Finley LW, Cross JR, Allis CD, Thompson CB. Intracellular alpha-ketoglutarate maintains the pluripotency of embryonic stem cells. Nature. 2014
23. Chin RM, et al. The metabolite alpha-ketoglutarate extends lifespan by inhibiting ATP synthase and TOR. Nature. 2014; 510:397–401. [PubMed: 24828042]
24. Ward PS, et al. Identification of additional IDH mutations associated with oncometabolite R(−)-2-hydroxyglutarate production. Oncogene. 2012; 31:2491–2498. [PubMed: 21996744]
25. Kranendijk M, et al. Evidence for genetic heterogeneity in D-2-hydroxyglutaric aciduria. Human mutation. 2010; 31:279–283. [PubMed: 20020533]
26. Ma S, et al. D-2-hydroxyglutarate is essential for maintaining oncogenic property of mutant IDH-containing cancer cells but dispensable for cell growth. Oncotarget. 2015; 6:8606–8620. [PubMed: 25825982]
27. Xu W, et al. Oncometabolite 2-hydroxyglutarate is a competitive inhibitor of alpha-ketoglutarate-dependent dioxygenases. Cancer cell. 2011; 19:17–30. [PubMed: 21251613]
28. Lawrence MS, et al. Discovery and saturation analysis of cancer genes across 21 tumour types. Nature. 2014; 505:495–501. [PubMed: 24390350]
29. Schmitz R, et al. Burkitt lymphoma pathogenesis and therapeutic targets from structural and functional genomics. Nature. 2012; 490:116–120. [PubMed: 22885699]
30. Kranendijk M, et al. IDH2 mutations in patients with D-2-hydroxyglutaric aciduria. Science. 2010; 330:336. [PubMed: 20847235]

31. Li C, et al. Copy number abnormalities, MYC activity, and the genetic fingerprint of normal B cells mechanistically define the microRNA profile of diffuse large B-cell lymphoma. Blood. 2009; 113:6681–6690. [PubMed: 19278952]
32. Rai D, Kim SW, McKeller MR, Dahia PL, Aguiar RC. Targeting of SMAD5 links microRNA-155 to the TGF-beta pathway and lymphomagenesis. Proc Natl Acad Sci U S A. 2010; 107:3111–3116. [PubMed: 20133617]
33. Qin Y, et al. Germline mutations in TMEM127 confer susceptibility to pheochromocytoma. Nat Genet. 2010; 42:229–233. [PubMed: 20154675]
34. Soding J, Biegert A, Lupas AN. The HHpred interactive server for protein homology detection and structure prediction. Nucleic acids research. 2005; 3:W244–w248. [PubMed: 15980461]
35. Arnold K, Bordoli L, Kopp J, Schwede T. The SWISS-MODEL workspace: a web-based environment for protein structure homology modelling. Bioinformatics. 2006; 22:195–201. [PubMed: 16301204]
36. Pettersen EF, et al. UCSF Chimera--a visualization system for exploratory research and analysis. Journal of computational chemistry. 2004; 25:1605–1612. [PubMed: 15264254]
37. Kim SW, et al. MicroRNAs miR-125a and miR-125b constitutively activate the NF-kappaB pathway by targeting the tumor necrosis factor alpha-induced protein 3 (TNFAIP3, A20). Proc Natl Acad Sci U S A. 2012; 109:7865–7870. [PubMed: 22550173]
38. Kim SW, Rai D, McKeller MR, Aguiar RC. Rational combined targeting of phosphodiesterase 4B and SYK in DLBCL. Blood. 2009; 113:6153–6160. [PubMed: 19369227]
39. Mullen AR, et al. Reductive carboxylation supports growth in tumour cells with defective mitochondria. Nature. 2012; 481:385–388. [PubMed: 22101431]
40. Contreras-Shannon V, Lin AP, McCammon MT, McAlister-Henn L. Kinetic properties and metabolic contributions of yeast mitochondrial and cytosolic NADP+-specific isocitrate dehydrogenases. The Journal of biological chemistry. 2005; 280:4469–4475. [PubMed: 15574419]
41. Koivunen P, et al. Transformation by the (R)-enantiomer of 2-hydroxyglutarate linked to EGLN activation. Nature. 2012; 483:484–488. [PubMed: 22343896]
42. Struys EA, Jansen EE, Verhoeven NM, Jakobs C. Measurement of urinary D- and L-2-hydroxyglutarate enantiomers by stable-isotope-dilution liquid chromatography-tandem mass spectrometry after derivatization with diacetyl-L-tartaric anhydride. Clinical chemistry. 2004; 50:1391–1395. [PubMed: 15166110]
43. Rakheja D, et al. Papillary thyroid carcinoma shows elevated levels of 2-hydroxyglutarate. Tumour biology : the journal of the International Society for Oncodevelopmental Biology and Medicine. 2011; 32:325–333. [PubMed: 21080253]
44. Rakheja D, Mitui M, Boriack RL, DeBerardinis RJ. Isocitrate dehydrogenase 1/2 mutational analyses and 2-hydroxyglutarate measurements in Wilms tumors. Pediatric blood & cancer. 2011; 56:379–383. [PubMed: 21225914]
45. Cheng T, et al. Pyruvate carboxylase is required for glutamine-independent growth of tumor cells. Proceedings of the National Academy of Sciences of the United States of America. 2011; 108:8674–8679. [PubMed: 21555572]

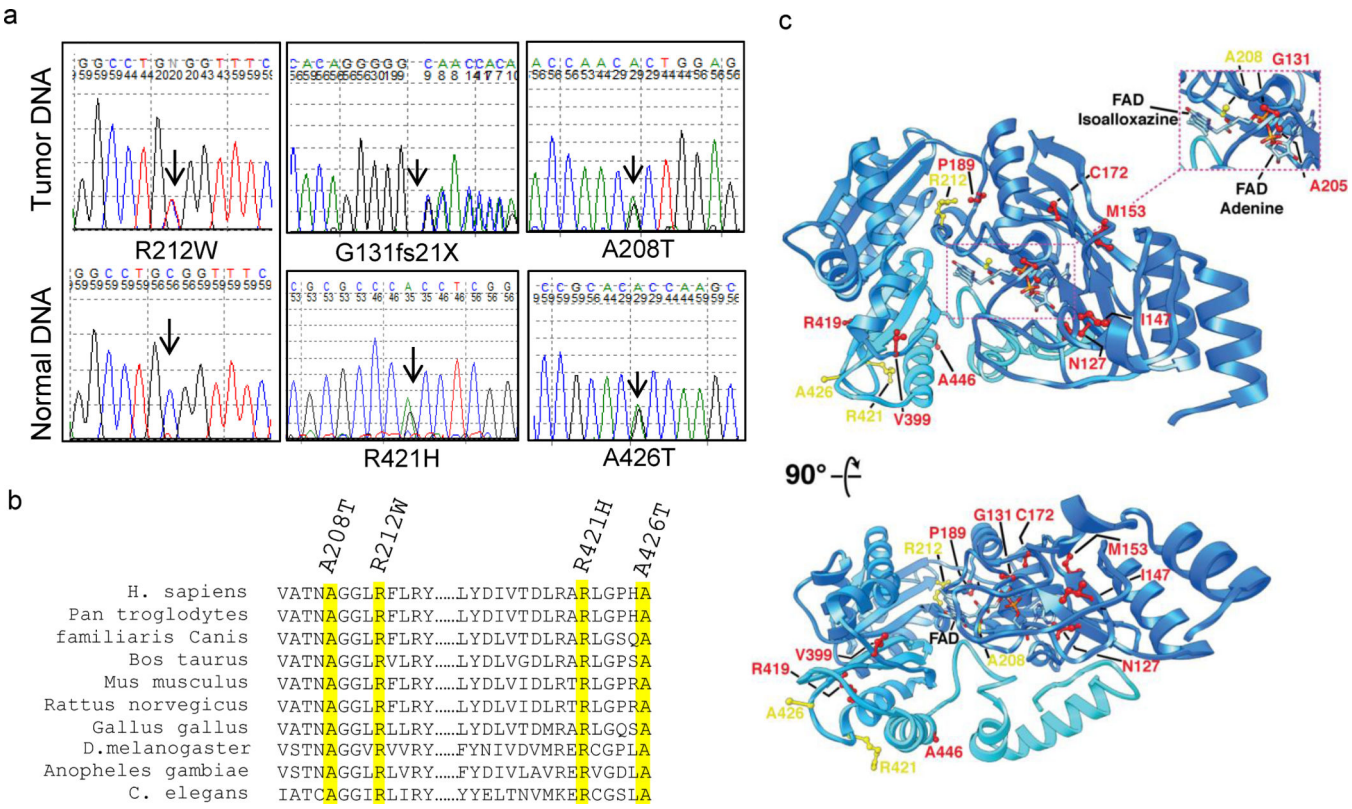

Figure 1. D2HGDH mutations in DLBCL

a) Sequencing traces representative of each of the five unique mutations found in DLBCL; arrows indicate the nucleotide change, and amino acid substitution is listed at the bottom. Constitutive DNA was available from two patients with D2HGDH mutant tumours (R212W variant), and one case is shown here. The G131fs21X, A208T and R421H mutations were found in cell lines, whereas A426T was found both in primary tumours and cell lines (Supplementary Table 1). **b)** All four missense variants identified in DLBCL map to fully conserved residues. **c)** Display of the closest structural homolog of human D2HGDH (dehydrogenase from Rhodopseudomonas palustris, PDB 3PM9) identified in the RCSB protein data bank. Orthogonal views of the structure are shown, with the non-covalently bound FAD displayed, as well as sidechains of the residues targeted by missense mutations in DLBCL (shaded yellow) or in D-2-hydroxyglutaric aciduria18 (shaded red). In both diseases, the mutations clustered to two structural areas - a region of possible contact with the FAD and/or the enzyme's substrate (see expansion subpanel), or an uncharacterized outside loop containing the residues V399, R419, R421, A426 and A446. The structures shown were generated using the program UCSF Chimera32.

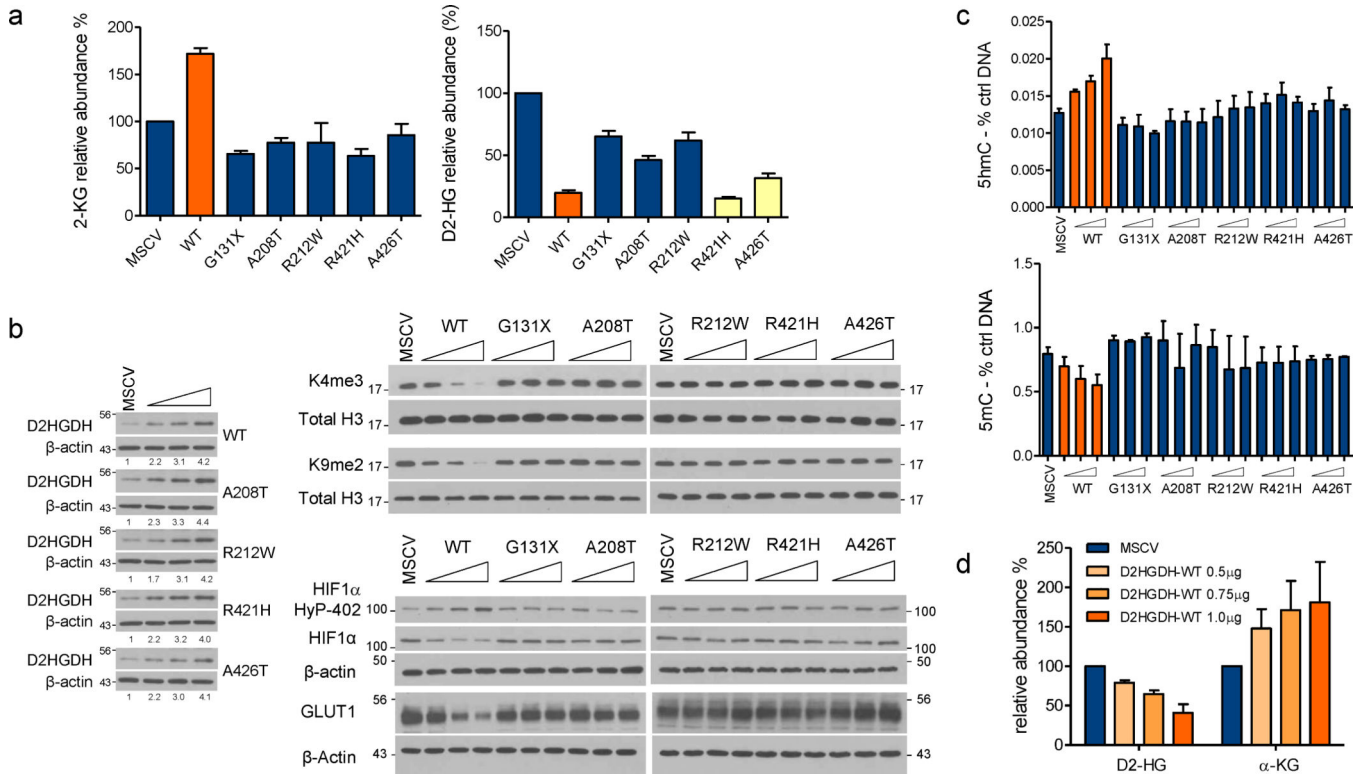

Figure 2. D2HGDH modulates D2-HG and α-KG levels and the read-out of dioxygenases function

a) Left: LC/MS show that WT-D2HGHD cells have significantly higher α-KG levels than empty-MSCV or mutant D2HGDH expressing isogenic cells ($p<0.0001$, ANOVA; $p<0.05$ Bonferroni's multiple comparison post-test). Right: expression of WT D2HGDH significantly lowered D2-HG levels in comparison to cells expressing and empty-MSCV or the G131X, A208T, and R212W mutants, but not R421H or A426T (yellow bars) ($p<0.0001$, ANOVA). **b)** Left: western blots of D2HGDH in cells transiently transfected with an empty vector (MSCV - 1μg) or increasing amounts (0.5μg, 0.75μg and 1μg) of the WT or mutant enzymes - densitometric quantification confirms the progressive elevation of D2HGDH levels. Right top: western blots of H3K4me3 and H3K9me2 show a progressive decrease in methylation in cells expressing the WT D2HGDH but not the mutant enzymes; right bottom: In hypoxia, expression of WT D2HGDH increases HIF1α hydroxylation (Pro-402), with decrease in its stability, and expression of the transcriptional target GLUT1; expression of mutant enzymes has no effects on HIF1α hydroxylation/expression. **c)** WT-D2HGDH cells display a significantly higher abundance of 5hmC marks (top panel, $p<0.0001$, ANOVA) and concomitant decrease in global DNA methylation (bottom panel, $p=0.035$, ANOVA). Expression of mutant D2HGDH did not significantly influence 5hmC or 5mC levels. **d)** Transient expression of WT D2HGDH significantly decreased D2-HG and increased α-KG levels in a dose-dependent manner ($p=0.006$ and $p=0.0002$, respectively, ANOVA). The data shown in a) represent the mean and SD of assays performed with four or five replicates per sample type, and displayed as relative levels to control cells (MSCV).. The transient transfection assays (b, c and d) were performed three to four times. The data shown in c) represent mean and SD of five data points derived from two biological

replicates. The data shown in d) represent the mean and SD of an assay performed in triplicate, displayed as relative levels to control cells (MSCV); the result from an independent biological replicate is shown in Supplementary Figure 6.

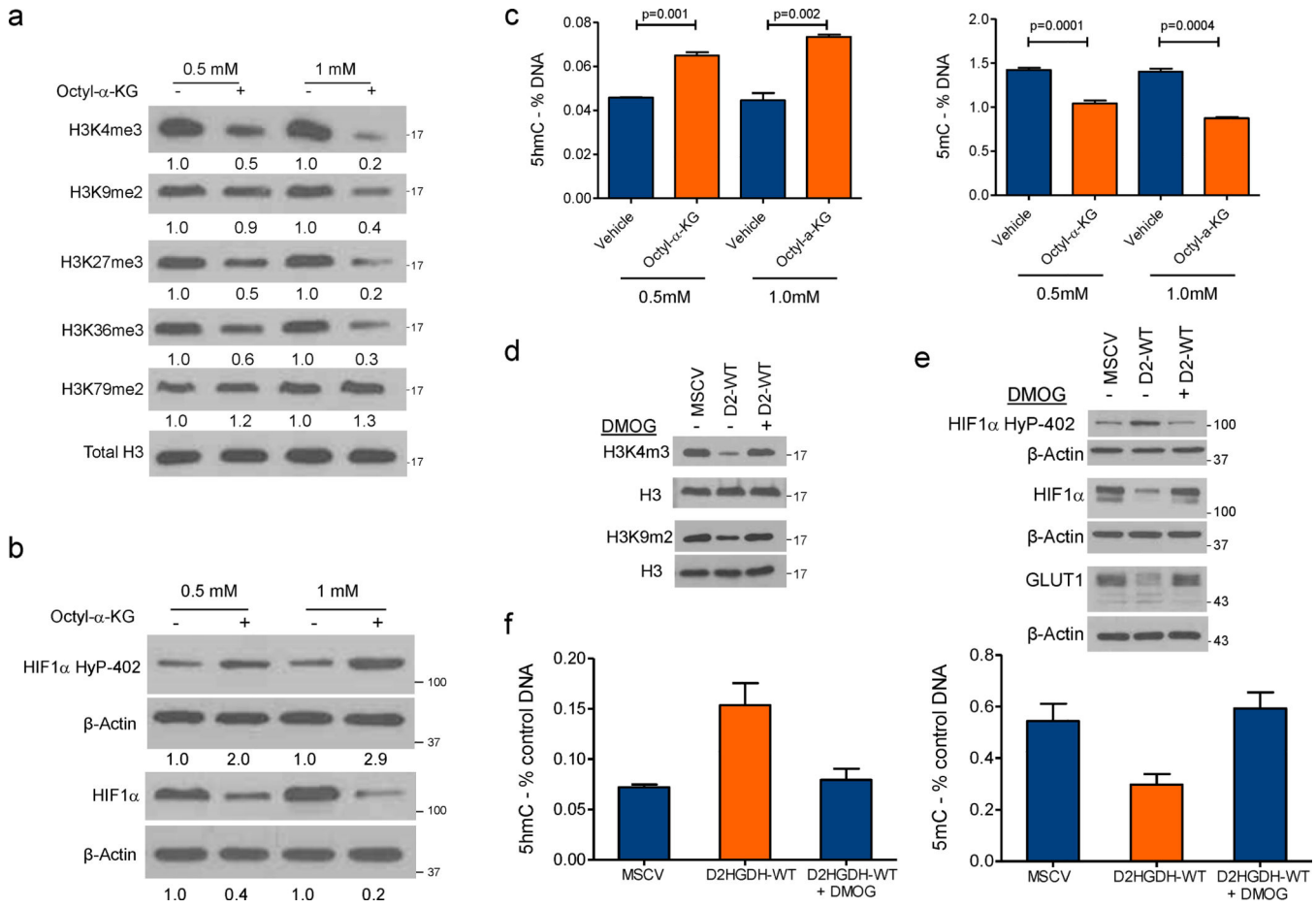

Figure 3. α-KG mediates the cellular effects of wild-type D2HGDH expression

a) Methylation of H3 lysine residues was determined by western blot in HEK-293 exposed to 0.5mM or 1mM of octyl-α-KG (or vehicle control) for 6h. Octyl-α-KG suppressed K4, K9, K27, K36 methylation in a dose-dependent manner. No changes were found in H3K79me2 levels confirming that this residue is not regulated by an α-KG-dependent HDM. **b)** Exposure to octyl-α-KG (or vehicle control) in cells grown under hypoxia (1% O_2) led to an increase in HIF1α hydroxylation (Pro-402) and consequent decrease in total HIF1α levels. Densitometric quantification is shown at the bottom of the western blots. **c)** Octyl-α-KG significantly increased the abundance of 5hmC marks in the DNA (p=0.0001, two-tailed Student's t-test, left panel) and decreased that of 5mC marks (global DNA methylation) (p=0.0001, two-sided Student's t-test, right panel), in a dose-dependent fashion. The data shown in c) represent the mean and SD of an assay performed in triplicate. Data shown in a-c were confirmed with at least one independent biological replicate. **d)** HEK-293 cells stably expressing WT D2HGDH were exposed to 1mM of dimethyloxalylglycine (DMOG) for 6h, and the methylation levels of H3 lysines verified by western blot. Exposure to DMOG restored K4me3 and K9me2 in D2HGDH-WT cells to the levels found in MSCV control. **e)** Hypoxia (1% O_2 for 18h) increases HIF1α hydroxylation (Pro402) and decreases its stability and activity, defined by GLUT1 expression, in cells expressing WT D2HGDH when compared to isogenic control cells (MSCV); exposure to DMOG fully countered the effects of WT D2HGDH on HIF1α and GLUT1. **f)** D2HGDH-

WT expressing cells display significantly higher and low abundance of 5hmC (left panel) and 5mC (right panel) marks, respectively, than its isogenic controls expressing an empty MSCV vector (p=0.0008 and p=0.0016 ANOVA). Exposure to DMOG (1mM for 6h) reversed the effects of WT D2HGDH back to the MSCV baseline. Experiments show in d and e were repeated twice, the data in f represent the mean and SD of a representative experiment (from two biological replicates) performed in triplicate.

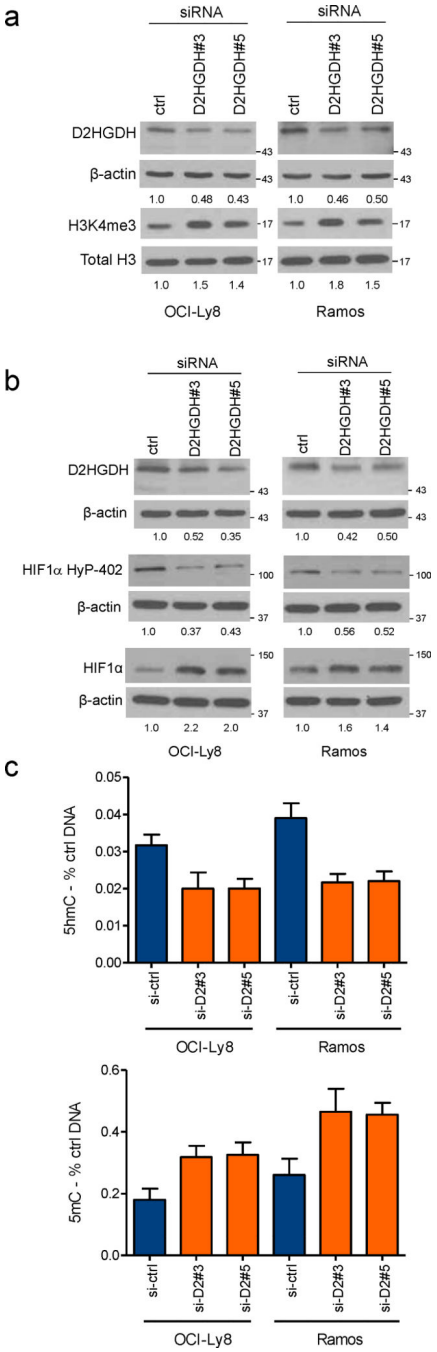

Figure 4. Partial knock-down of D2HGDH in B cell lymphoma cell lines significantly modifies histone/DNA methylation and HIF1α hydroxylation

a) SiRNA-mediated partial knockdown of D2HGDH with two targeting oligonucleotides increased the methylation levels of H3K4me3 in comparison to cells transfected with a control siRNA. **b)** Under hypoxia (1% O2, 16h), B lymphoma cells with partial suppression of D2HGDH expression displayed lower HIF1α hydroxylation and consequent stabilization of total HIF1α. In a) and b), the extent of D2HGDH suppression is shown by western blotting and densitometry quantifies all relevant changes. **c)** The levels of 5hmC and 5mC (top and bottom panels), were significantly lower and higher, respectively, in cells with a

D2HGDH KD when compared to their isogenic controls ($p<0.0001$, ANOVA, $p<0.05$ Bonferroni's Multiple Comparison Test for si-ctrl vs. si-D2#3 or siD2#5). The 5hmC and 5mC measurements shown are the mean and SD of three data points derived from three biological replicates. The transient knockdown of D2HGDH in these cell lines was repeated three times.

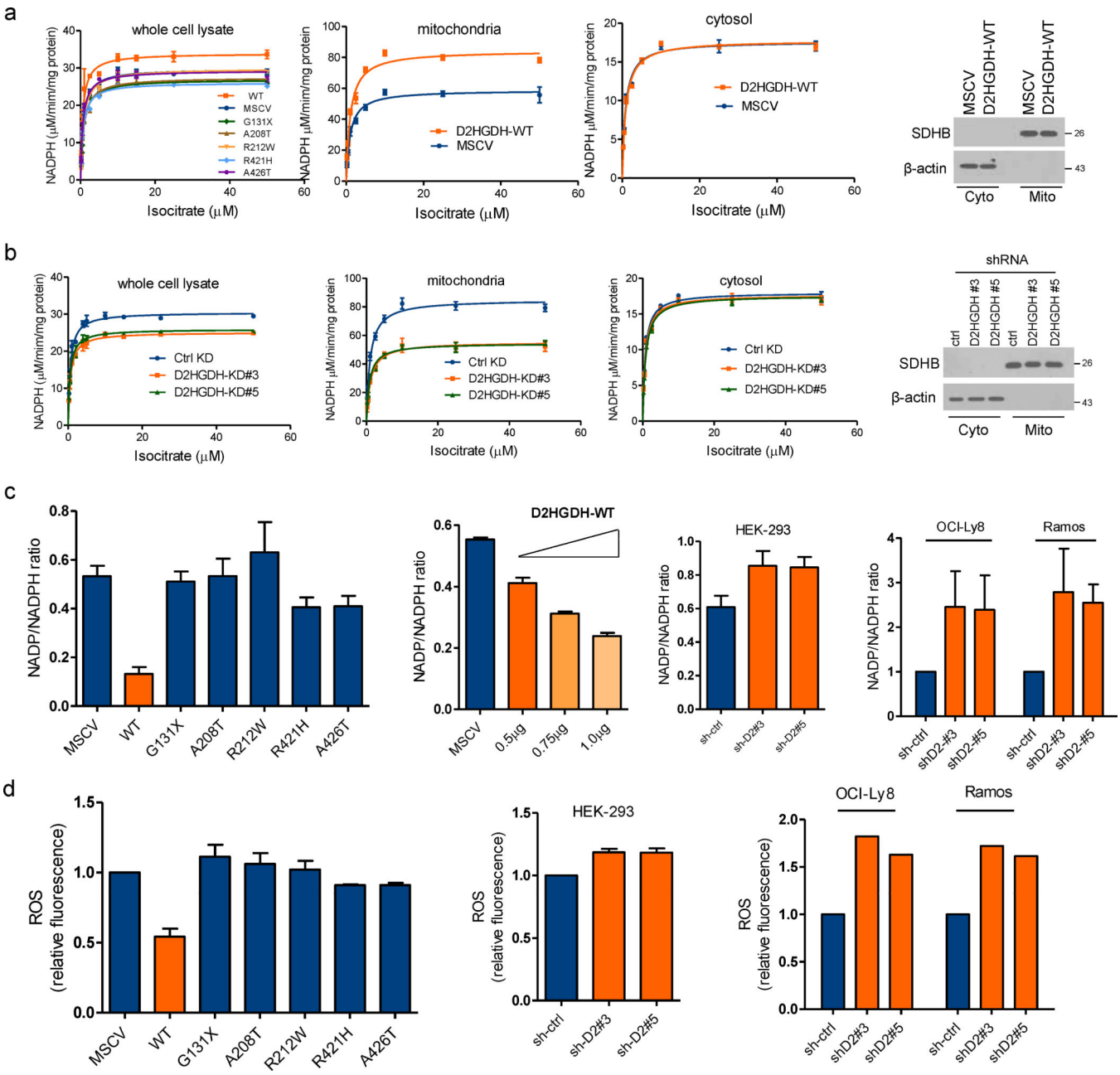

Figure 5. D2HGDH expression influences mitochondrial IDH activity and the cellular redox state

a) Left panel: HEK-293 cells stably expressing WT D2HGDH displayed a significantly higher V_{max} for IDH than those expressing mutant D2HGDH or an empty vector ($p<0.0001$, ANOVA). **Middle panels**: subcellular fractionation demonstrates that D2HGDH increases the V_{max} for IDH in the mitochondria, but not in the cytosol; western blots at the right confirm the efficacy of the subcellular separation. **b) Left panel**: knockdown of D2HGDH significantly decreased the V_{max} for IDH ($p<0.0001$, ANOVA). **Middle panels**: subcellular fractionation demonstrates that D2HGDH levels influences exclusively the V_{max} for mitochondrial IDH. Western blots at the right confirm the purity of the subcellular fractions.

The data are shown as a non-linear regression (curve fit) and panel represents mean ± SD of an assay performed in triplicate. Together with the data shown in Supplementary Figure 9, the effects of D2HGDH on IDH activity were confirmed in three independent models of D2HGDH KD and two models of D2HGDH ectopic expression. The enzyme kinetics was calculated with the Michaelis-Menten equation. **c) Left:** expression of WT D2HGDH significantly lowered NADP/NADPH ratio in comparison to isogenic cells expressing mutant D2HGDH or an empty vector ($p=0.017$, ANOVA), data show are mean ± SD from two biological replicates. **Middle:** Transient expressionof WT D2HGDH significantly lowered the NADP/NADPH ratio ($p<0.0001$, ANOVA); data shown are mean ± SD of an assay performed in triplicate. **Right panels**: Stable (HEK-293) or transient (OCI-Ly8 and Ramos) knockdown of D2HGDH significantly increased NADP/NADPH ratio ($p=0.01$ and $p=0.003$, ANOVA, for HEK-293 or OCI-Ly8 and Ramos, respectively). Data shown are mean ± SD of three biological replicates. **d) Left:** cells expressing WT D2HGDH displayed significantly lower ROS levels than the isogenic models of mutant D2HGDH or empty-MSCV ($p=0.0002$, ANOVA); data show are mean ± SD from two biological replicates. Stable (**middle**) or transient (**right**) KD of D2HGDH in three distinct cell models significantly increased ROS levels ($p=0.007$, ANOVA, for all comparisons). Data shown at the middle are from two biological replicates; data on the right are from a single assay. In all instances, the Bonferroni's Multiple Comparison post-hoc test yielded a $p<0.05$).

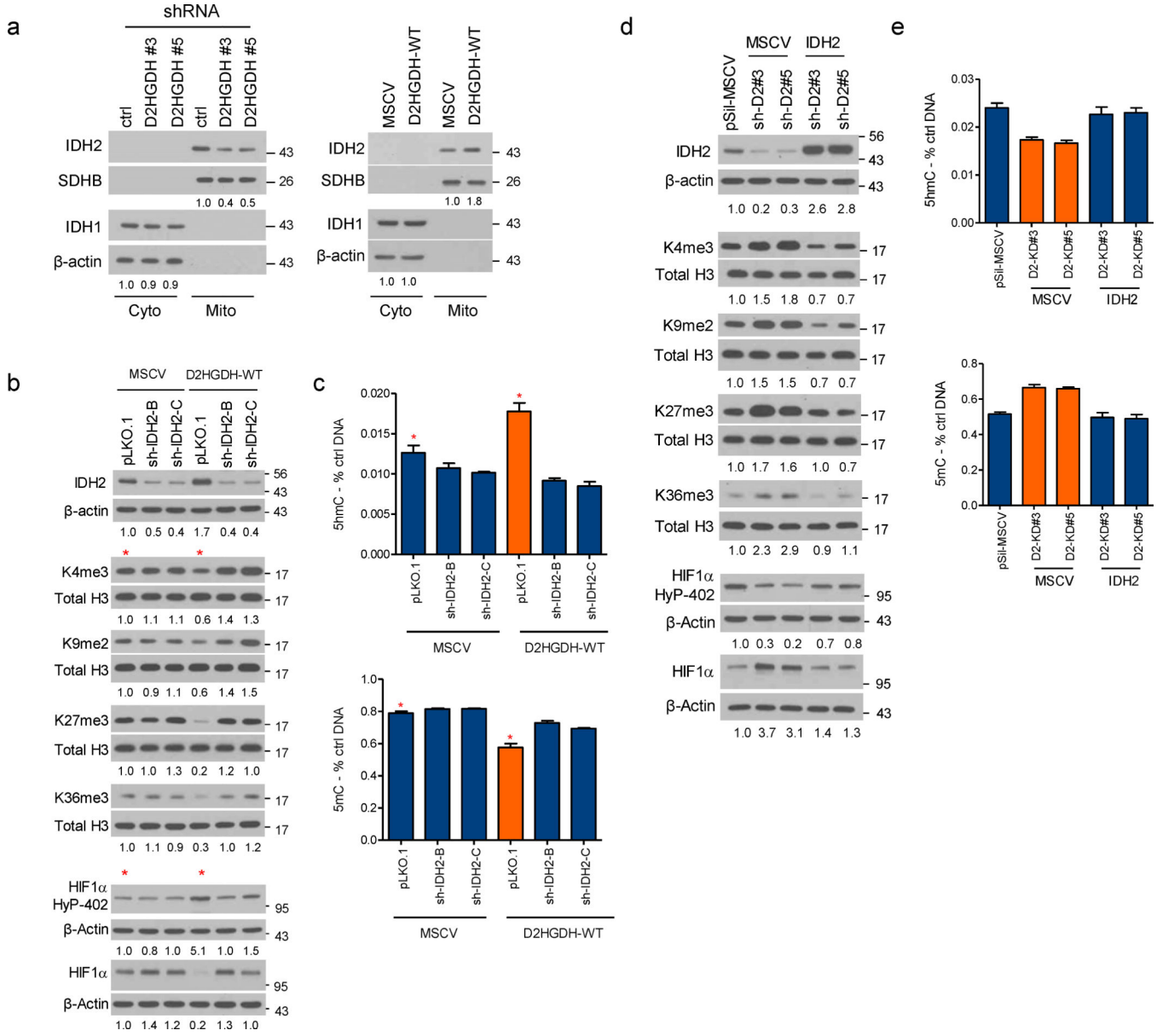

Figure 6. IDH2 mediates D2HGDH effects on histone and DNA methylation and HIF1α hydroxylation

a) Western blot analysis of IDH1 and IDH2 in subcellular fractions of D2HGDH models (knockdown, left panel; ectopic expression, right panel) shows modulation of IDH2 levels. Densitometric quantification is shown at the bottom. **b)** Top – western blot analysis of IDH2-KD cells expressing an empty-MSCV vector or WT D2HGDH. Middle – Expression of WT D2HGDH decreased H3K methylation (compare lanes marked with a red star); IDH2 KD restored the H3K methylation levels in these cells. Bottom - expression of WT D2HGDH increased HIF1α hydroxylation and decreased total HIF1α levels (compare lanes marked with a red star); IDH2 KD reversed the increase in HIF1α hydroxylation (and decrease in total HIF1α) associated with expression of D2HGDH WT. **c)** Cells expressing D2HGDH-WT (and an empty pLKO.1) displayed a significantly higher abundance of 5hmC

marks (top) and a concomitant decrease in global DNA methylation (botton) than MSCV-pLKO.1 controls (marked by red star; $p<0.001$ two-tailed, Student's t-test). IDH2 KD significantly lowered or increased the levels of 5hmC and 5mC marks, respectively, in D2HGDH-WT cells ($p<0.0001$, ANOVA, $p<0.001$ Bonferroni's Multiple Comparison Test), with a more modest change in MSCV-expressing controls. These data are mean and SD of an assay performed in triplicate, which was confirmed in an independent biological replicate. The data from the WBs were confirmed in two to three biological replicates. **d)** Top - western blot analysis of IDH2 ectopic expression in D2HGDH-KD cells. Middle – D2HGDH KD elevated H3K methylation (compare the three first lanes) and this change was abrogated by expression of IDH2. Bottom – D2HGDH KD decreased HIF1α hydroxylation and increased its total levels (compare the three first lanes); these changes were absent in D2HGDH KD cells ectopically expressing IDH2. **e)** D2HGDH KD decreased the abundance of 5hmC marks (top) and increased global DNA methylation 5mC (bottom) (<0.0001, ANOVA); expression of IDH2 restored these values to that of control (pSIL-MSCV) isogenic cells. These data are mean and SD of an assay performed in triplicate, confirmed in a biological replicate. The western blot data shown in d) were confirmed in biological replicates.

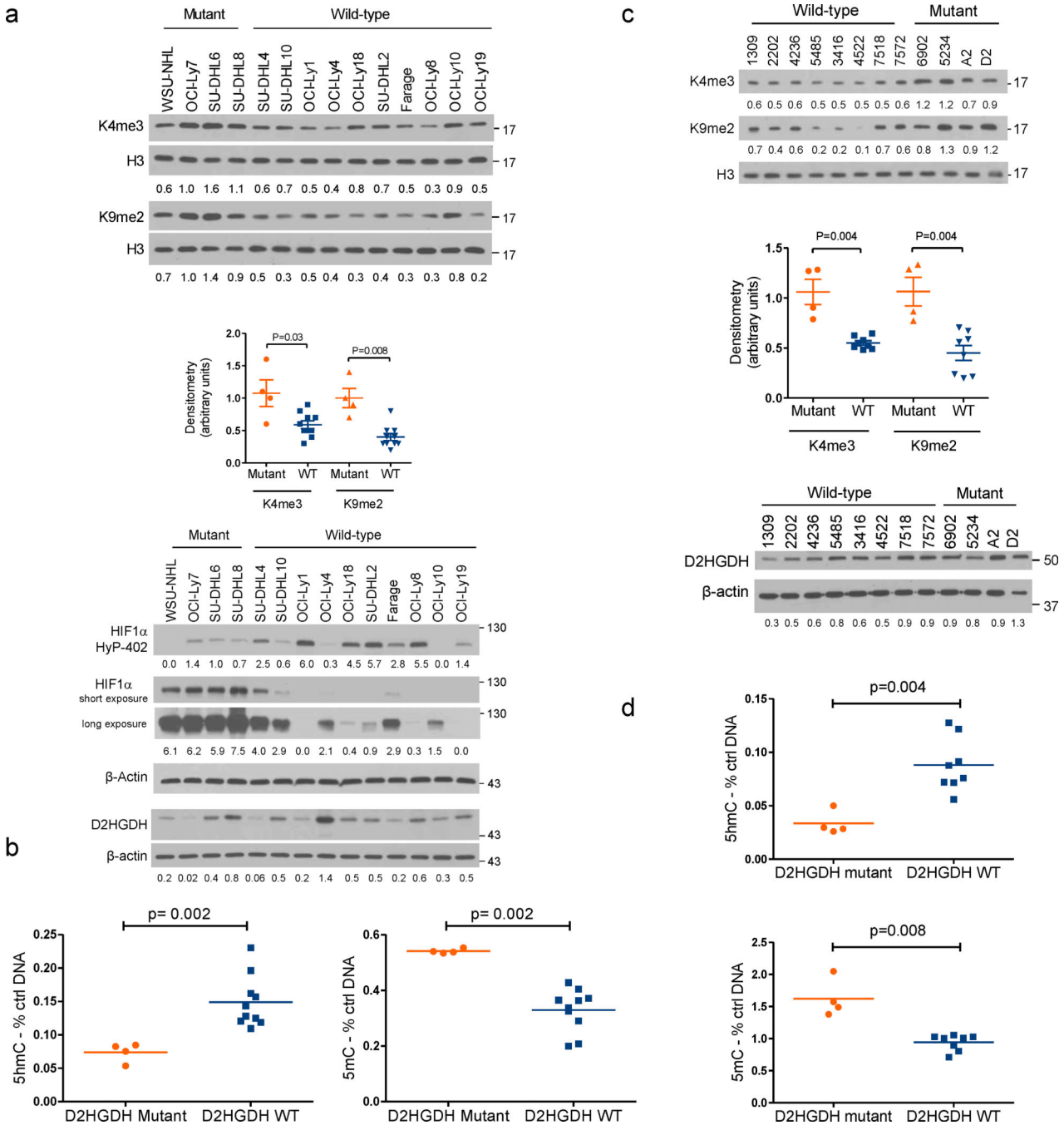

Figure 7. Cellular effects of *D2HGDH* mutations in DLBCL

a) Methylation of H3 lysine residues, and HIF1α hydroxylation/total levels (under hypoxic conditions) were determined by western blot in 14 DLBCL cell lines. H3K4 and K9 methylation were higher, while HIF1α hydroxylation (Hy-HIF1α) was lower (and its total levels consequently higher) in D2HGDH-mutant cell lines when compared to those expressing the WT enzyme. Densitometric quantifications are shown at the bottom of the western blots, and for H3K4me3 and H3K9me2 also in graphic display (mean and SEM, Mann-Whitney test). The WB at the bottom displays the expression of D2HGDH across

these cell lines. **b)** The levels of 5hmC marks and the global DNA methylation were significantly lower and higher, respectively, in DLBCL cell lines expressing a mutant D2HGDH gene than in the WT cells (p=0.002, two-tailed Mann-Whitney test). The data shown are mean of 3 data points for each cell line (4 mutant, 10 WT) derived from three independent biological replicates. **c)** Western blot analysis of 12 primary DLBCLs (four mutant and eight D2HGDH WT) shows higher H3K4 and H3K9 methylation in mutant lymphomas. Densitometric quantification of H3K4me3 and H3K9me2 (normalized by total H3) is shown below the blots and in graphic display (mean and SEM,Mann-Whitney test). The WB at the bottom shows the expression of D2HGDH across these biopsies. **d)** The levels of 5hmC marks and the global DNA methylation were significantly lower and higher, respectively, in DLBCLs expressing a mutant D2HGDH gene than in the WT cells (p=0.004 or 0.008, two-tailed Mann-Whitney test). The data shown are mean of 3 independent measurements for each tumour